Observation of high-frequency electrostatic waves in the vicinity of the reconnection ion diffusion region by the spacecraft of the Magnetospheric Multiscale (MMS) mission

M. Zhou, M. Ashour-Abdalla, J. Berchem, R. J. Walker, H. Liang, M. El-Alaoui, M. L. Goldstein, P. -A. Lindqvist, G. Marklund, Y. V. Khotyaintsev, et al.

AGU PUBLICATIONS

Geophysical Research Letters

RESEARCH LETTER
10.1002/2016GL069010

Special Section:
First results from NASA's Magnetospheric Multiscale (MMS) Mission

Observation of high-frequency electrostatic waves in the vicinity of the reconnection ion diffusion region by the spacecraft of the Magnetospheric Multiscale (MMS) mission

M. Zhou[1], M. Ashour-Abdalla[1], J. Berchem[1], R. J. Walker[2], H. Liang[1], M. El-Alaoui[1], M. L. Goldstein[3], P.-A. Lindqvist[4], G. Marklund[4], Y. V. Khotyaintsev[5], R. E. Ergun[6], F. D. Wilder[6], C. T. Russell[2], R. J. Strangeway[2], C. Zhao[2], W. R. Paterson[3], B. L. Giles[3], C. J. Pollock[3], R. B. Torbert[7], J. L. Burch[8], J. C. Dorelli[3], D. J. Gershman[3], L. A. Avanov[3], B. Lavraud[9,10], and M. O. Chandler[11]

[1]Department of Physics and Astronomy, University of California, Los Angeles, California, USA, [2]Department of Earth, Planetary, and Space Sciences, University of California, Los Angeles, California, USA, [3]NASA, Goddard Space Flight Center, Greenbelt, Maryland, USA, [4]Royal Institute of Technology, Stockholm, Sweden, [5]Swedish Institute of Space Physics, Uppsala, Sweden, [6]LASP, University of Colorado Boulder, Boulder, Colorado, USA, [7]Department of Physics, University of New Hampshire, Durham, New Hampshire, USA, [8]Southwest Research Institute, San Antonio, Texas, USA, [9]Institut de Recherche en Astrophysique et Planétologie, Toulouse, France, [10]Centre National de la Recherche Scientifique, Toulouse, France, [11]NASA Marshall Space Flight Center, Huntsville, Alabama, USA

Key Points:
- Ion diffusion region was identified by MMS spacecraft in the Earth's dayside magnetopause
- High-frequency electrostatic waves were observed in the vicinity of the ion diffusion region
- Energy dissipated by these high-frequency waves is negligible compared to that by the lower-frequency process

Correspondence to:
M. Zhou,
mzhou@physics.ucla.edu

Citation:
Zhou, M., et al. (2016), Observation of high-frequency electrostatic waves in the vicinity of the reconnection ion diffusion region by the spacecraft of the Magnetospheric Multiscale (MMS) mission, *Geophys. Res. Lett.*, *43*, 4808–4815, doi:10.1002/2016GL069010.

Received 5 APR 2016
Accepted 10 MAY 2016
Accepted article online 12 MAY 2016
Published online 27 MAY 2016

Abstract We report Magnetospheric Multiscale observations of high-frequency electrostatic waves in the vicinity of the reconnection ion diffusion region on the dayside magnetopause. The ion diffusion region is identified during two magnetopause crossings by the Hall electromagnetic fields, the slippage of ions with respect to the magnetic field, and magnetic energy dissipation. In addition to electron beam modes that have been previously detected at the separatrix on the magnetospheric side of the magnetopause, we report, for the first time, the existence of electron cyclotron harmonic waves at the magnetosheath separatrix. Broadband waves between the electron cyclotron and electron plasma frequencies, which were probably generated by electron beams, were found within the magnetopause current sheet. Contributions by these high-frequency waves to the magnetic energy dissipation were negligible in the diffusion regions as compared to those of lower-frequency waves.

1. Introduction

How magnetic energy dissipates and how particles are accelerated remain two fundamental outstanding questions of magnetic reconnection. Plasma waves may contribute significantly to these two processes by providing the necessary anomalous resistivity to break the magnetic field lines and/or accelerate electrons to suprathermal energy through Landau resonance [*Treumann*, 2001; *Zhou et al.*, 2014]. Different types of waves have been associated with magnetic reconnection. Many of them, such as lower hybrid waves, whistler waves, and electrostatic solitary waves, have been observed near the reconnection separatrices [*Deng et al.*, 2004; *Vaivads et al.*, 2004; *Retino et al.*, 2006; *Zhou et al.*, 2011; *Viberg et al.*, 2013; *Graham et al.*, 2016]. In particular, *Vaivads et al.* [2004] found Langmuir waves on the magnetosphere and magnetosheath separatrices of a magnetopause reconnection region. *Retino et al.* [2006] revealed the different features of waves and particles observed by Cluster when crossing the magnetospheric separatrix at the dayside magnetopause. In addition, whistler waves and electrostatic electron cyclotron waves have been observed inside the electron diffusion region at the magnetopause [*Tang et al.*, 2013]. An important feature of the dayside magnetospheric boundary is that plasma density and temperature, as well as the magnetic field strength, differ substantially across the magnetopause, which leads to a substantial asymmetry in the reconnection process across the boundary layer (see review by *Mozer and Pritchett* [2010]).

In this letter, we report observations of high-frequency electrostatic waves that were made by the spacecraft of NASA's Magnetospheric Multiscale (MMS) mission on 3 October 2015. During that day, the spacecraft encountered the ion diffusion region of a reconnection event in the postnoon region of the dayside magnetopause. The unprecedented temporal and spatial resolutions of the instruments on board MMS enable us to establish that the spacecraft crossed the ion diffusion region. We describe below the characteristics of the

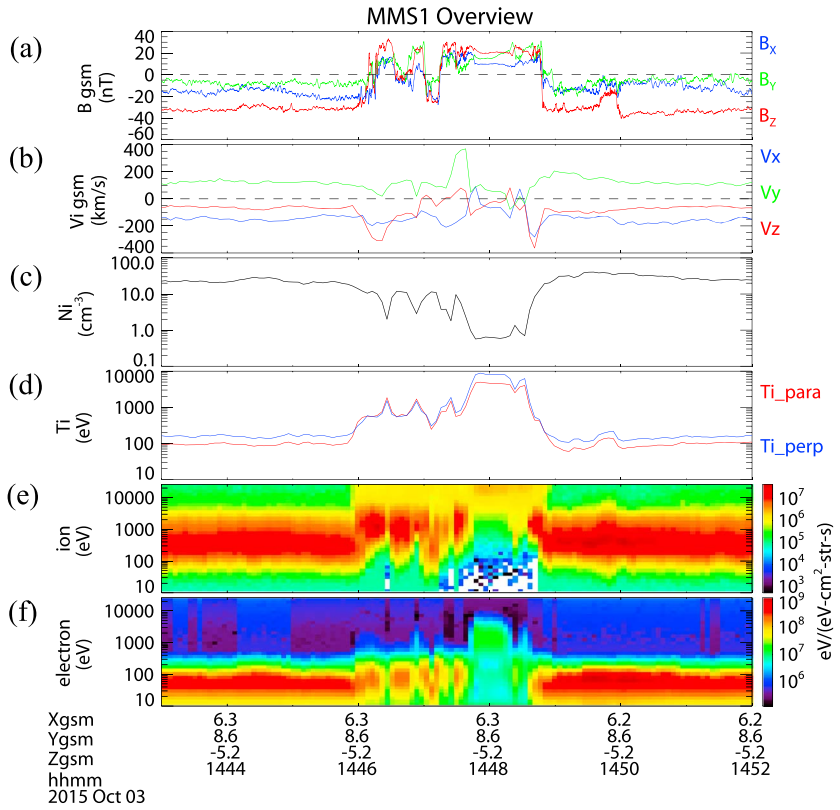

Figure 1. An overview of MMS1 observations in the fast survey mode during 14:43–14:52 UT on 3 October 2015. (a) Magnetic field components, (b) ion bulk velocity components, (c) ion density, (d) ion temperatures parallel (red) and perpendicular (blue) to the magnetic field, and (e and f) ion and electron differential energy fluxes, respectively. Vectors are shown in the GSM coordinates.

waves observed in the separatrices and the magnetopause current sheet and relate them to the energy dissipation occurring during magnetic reconnection.

2. Instrumentation

The main goal of the four-spacecraft constellation of MMS that was launched on 12 March 2015 is to investigate magnetic reconnection along the dayside magnetopause and in the neutral sheet of the magnetotail [*Burch et al.*, 2015]. The data used in our study were acquired when MMS was in the burst mode, which consists of only a few percent of operation time but makes up more than 70% of the data. The Fluxgate Magnetometer provides three-dimensional magnetic fields with cadence of 128 samples/s in the burst mode and 8 samples/s in the fast survey mode [*Russell et al.*, 2014; *Torbert et al.*, 2014]. The Electric Double Probe (EDP) provides three-dimensional electric fields with a cadence of 128 samples/s in the burst mode. It also provides short bursts of 65,536 samples/s electric fields [*Lindqvist et al.*, 2014; *Ergun et al.*, 2014; *Torbert et al.*, 2014]. The Fast Plasma Instrument (FPI) provides 3-D electron distributions with a time resolution of 30 ms and ion distributions with a time resolution of 150 ms. The energy ranges of FPI are from 10 eV to 30 keV for both electrons and ions. Plasma moments (density, velocity, temperature, etc.) integrated by using the full distributions are also provided with the same cadence [*Pollock et al.*, 2016].

3. Event Overview

MMS skimmed the postnoon magnetopause between 14:46 and 14:49 UT on 3 October 2015. The position of MMS was [6.3, 8.6, −5.2] R_E at 14:46 UT in geocentric solar magnetospheric (GSM) coordinates. The four spacecraft formed a tetrahedron in space with an average distance of 25 km between spacecraft. Figure 1 shows an overview of MMS1 observations between 14:43 and 14:52 UT. MMS1 was in the magnetosheath

before 14:46 UT. It then encountered the magnetopause (MP) current sheet several times. After 14:49 UT, it returned to the magnetosheath which was characterized by high plasma density (~40/cm^3) and low ion temperature (~100 eV). Magnetic field strengths on the two sides of the current layer were very similar, but plasma density and temperature differed by a factor of 30.

The six MP crossings are characterized by reversals of the magnetic field B_z component and variations in the ion density and temperature between 14:46 UT and 14:49 UT. During the first crossing MMS1 did not enter the magnetosphere proper since the density and temperature did not reach the magnetospheric levels observed shortly afterward. The magnitudes of the ion density and temperature were in between magnetosphere and magnetosheath values, and thus, MMS1 was probably in the low-latitude boundary layer. The crossing at around 14:47 UT was also a partial crossing. After 14:47:20 UT, MMS moved to the magnetosphere proper as the ion density dropped down to 1/cm^3 and the temperature went up to 8 keV.

4. Ion Diffusion Region

Below we examine two MP crossings between 14:46:50 and 14:47:20 UT. For convenience we call the former MP crossing MP1 and the latter MP2. In this section we show that ion diffusion regions were detected during both crossings. Figures 2a–2g display the detailed structures of MP1, while Figures 2i–2n show the data for MP2. Figures 2h and 2o show the 2-D schematics of MMS trajectories through the diffusion region around the X line. We have transformed the vectors into local boundary normal coordinates, which were determined by a minimum variance analysis (MVA) of the magnetic fields [*Sonnerup and Scheible*, 1998]. *N* points outward along the MP normal, *L* is the maximum variation direction and points along the reconnecting magnetic field component, and *M* completes a right-handed orthogonal coordinate system. The transformation from GSM coordinates to current sheet normal coordinates for MP1 is given by $L = [0.279, 0.667, 0.691]$, $M = [0.237, -0.745, 0.624]$, and $N = [0.931, -0.011, -0.366]$ by applying a MVA of the magnetic field data between 14:46:56 and 14:47:07 UT. The current sheet normal coordinates for MP2 is $L = [0.599, 0.374, 0.708]$, $M = [0.675, 0.241, -0.698]$, and $N = [-0.431, 0.896, -0.108]$ by applying a MVA of the magnetic field data between 14:47:10 and 14:47:20 UT. The MP normal *N* inferred from four spacecraft timing analysis is $N = [0.859, 0.032, -0.512]$ for MP1 and $N = [-0.058, 0.937, -0.345]$ for MP2 [*Sonnerup et al.*, 2008]. These two normals are consistent with those inferred from MVA. MP thicknesses were estimated by multiplying the MP speed by the crossing duration that was defined as the time between the measurements of the two asymptotic B_L values. The thicknesses of MP1 and MP2 are 220 km and 440 km, that is, 4.5 $d_{i,\mathrm{hybrid}}$ and 10.7 $d_{i,\mathrm{hybrid}}$, respectively. Here $d_{i,\mathrm{hybrid}}$ is the hybrid ion inertial length between the magnetosphere values and the magnetosheath values. Ion inertial length is determined by $c/\sqrt{ne^2/\varepsilon 0 m_i}$, where *c* is the light speed, *n* is the density, *e* is the charge, m_i is the mass of the ion, and ε_0 is the vacuum dielectric constant.

Figure 2b shows that the flow velocity along the *L* direction (V_L) reversed at the MP1 crossing, the negative speed being about 150 km/s larger than the positive speed. By using a timing analysis based on flow reversal times from all four spacecraft, we estimated that the X line moved along the $-L$ direction with a speed of ~60 km/s. The maximum flow speeds on the two sides of the X line were approximately 170 km/s and 190 km/s, respectively, in the X line reference frame. *Cassak and Shay* [2007] have shown that for asymmetric reconnection the outflow speed scales like the hybrid Alfvén speed that is based on the combination of the geometric and arithmetic means of the field and densities on each side the current sheet. Since the predicted hybrid Alfvén speed is about 210 km/s, the observed outflow speeds are about 80% of the theoretical values expected for magnetic reconnection. Similarly, the maximum outflow speed is 180 km/s for MP2, which is about 75% of the predicted Alfvén speed, suggesting that the observed flows were caused by reconnection.

To examine in detail the electromagnetic field structure for MP1, we calculated the perpendicular electric field in the ion frame $E' = E_{\mathrm{perp}} + V_i \times B$ (Figure 2c). E_{perp} was calculated from the two in-plane components by assuming that there was no parallel electric field, i.e., $E \cdot B = 0$. To avoid large uncertainties we calculated E_{perp} only in regions where $|B| > 2$ nT and the angle between *B* and the spin plane was larger than 15°. Figure 2c shows that all three components of *E*′ deviate from zero during the crossing. This behavior indicates a slippage of ions from the magnetic field [*Dai et al.*, 2015; *Goldman et al.*, 2015]. Near the reversal of B_L, B_M also reverses from negative to positive with a peak-to-peak magnitude of about 20 nT; meanwhile E_N' reverses from positive to negative. A MMS trajectory superimposed over a sketch of a 2-D model is shown in

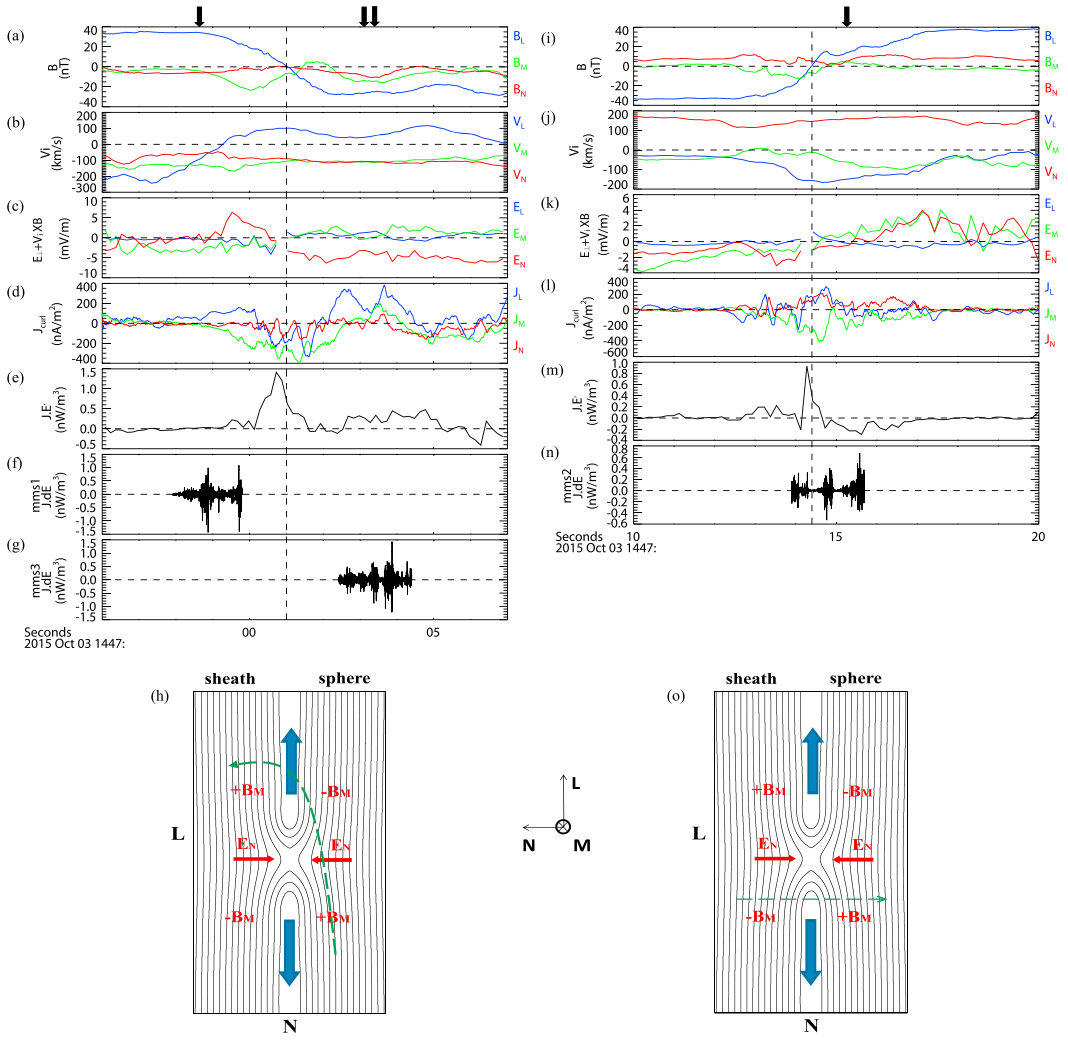

Figure 2. Ion diffusion regions observed by MMS using the burst mode data: (a) magnetic field components, (b) ion bulk velocity components, (c) electric fields in the ion frame, (d) electric current density, (e) magnetic energy dissipation rate from the lower-frequency electromagnetic fields $J \cdot (E_{perp} + V_i \times B)$, and (f) high-frequency electrostatic waves. Figures 2a–2g are for MP1 observed by MMS1, and Figures 2i–2n are for MP2 observed by MMS2. Figures 2h and 2o are the 2-D schematics of MMS trajectories through the ion diffusion region. Dashed green traces represent the MMS trajectories. Blue arrows on top of Figures 2a and 2i mark the times of the waveforms shown in Figure 3. We should note that the dissipation contributed by high-frequency waves were calculated using the data from individual spacecraft while $J \cdot (E_{perp} + V_i \times B)$ was calculated using the data from all four spacecraft.

Figure 2h. It suggests that MMS moved from southward to northward of the X line and then crossed the current sheet from the magnetosphere to the magnetosheath northward of the X line. The perturbations of B_M and E_N' along the MMS trajectory are consistent with the polarities of the Hall fields of collisionless reconnection depicted in Figure 2h. Numerical simulations of reconnection with a density asymmetry across a current sheet [e.g., *Tanaka et al.*, 2008] have shown that the quadrupolar out-of-plane Hall magnetic field is replaced by a bipolar Hall magnetic field on the magnetosheath side and the bipolar Hall electric field normal to the current sheet is replaced by a unipolar electric field on the magnetosphere side. However, *Pritchett* [2008] showed that quadrupolar Hall magnetic fields and bipolar Hall electric fields were robust features of the magnetopause current sheet in a simulation with external driving at the magnetosheath side inflow boundaries.

MP2 was observed during an inbound crossing from the magnetosheath to the magnetosphere. Plasma flow V_L was opposite to that during the MP1 crossing. B_M changed from negative to positive as B_L changed from negative to positive. E_N' was mostly negative on the magnetosheath side and positive in the magnetosphere.

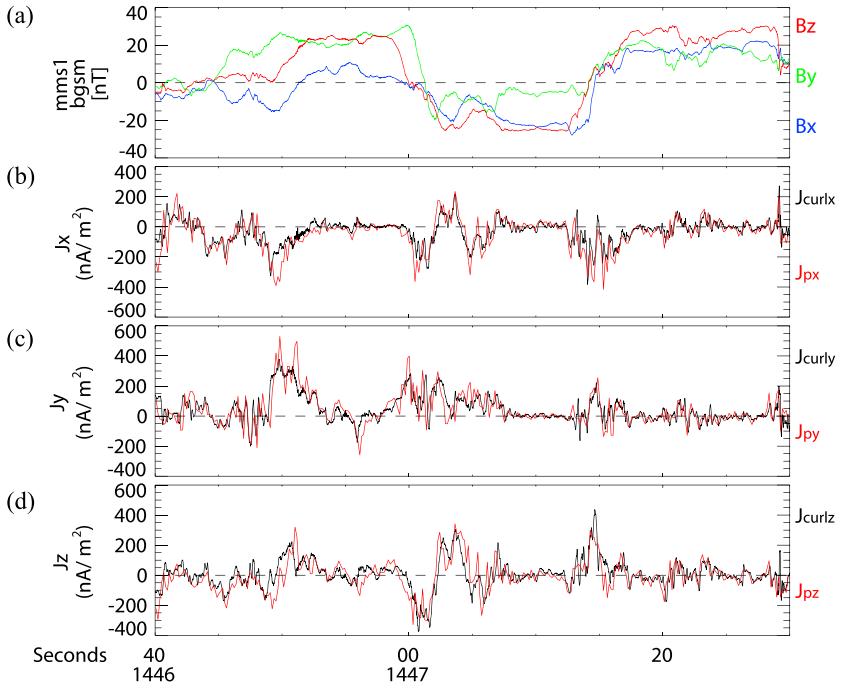

Figure 3. Comparison of current density derived from Ampere's law and from plasma moments for MMS1. (a–d) Three components of magnetic fields, current density J_x, J_y, and J_z. Black traces represent the current density computed using the curlometer method, while red traces indicate the current density computed from plasma moments.

These features are signatures of the Hall magnetic and electric fields expected for fast magnetic reconnection mediated by whistler waves or kinetic Alfvén waves [*Dai*, 2009]. All three components of E' deviate from zero within the Hall region as they did for MP1.

Figures 2e and 2m display $J \cdot E'$ as a measure of the energy dissipation rate for the two MP crossings, respectively. J is the electric current density calculated by the curlometer method [*Dunlop et al.*, 2002] (shown in Figures 2d and 2l), assuming that the current is uniform within the tetrahedron. Figure 3 provides the comparison between the electric current density calculated by the curlometer method and that derived from plasma moments ($J = n_i e(V_i - V_e)$) for MMS1. We find that the current densities computed from the two methods are in good agreement with each other, indicating that electric current density can be accurately calculated by individual spacecraft. Current densities derived from plasma moments from other three spacecraft are similar to that calculated by MMS1 and are consistent with current density calculated by the curlometer method (not shown). There are a few discrepancies that might be due to small-scale current filaments that can only be resolved by individual spacecraft. The dissipation regions are indicated by $J \cdot E' > 0$. The most prominent energy dissipation occurred around $B_L = 0$ for both crossings. For MP1 the dissipation region extended to the magnetosheath separatrix, while it was mostly located on the magnetosheath side for MP2 with a dynamo region ($J \cdot E' < 0$) on the magnetospheric side of the current sheet. We should note that the crossing times of the dissipation regions were less than 2 s and thus could not have been resolved by particle instruments on previous missions. Combining all of the above evidence, we conclude that MMS detected ion diffusion regions during both crossings.

5. High-Frequency Waves

Figure 4 presents four typical waveforms and corresponding power spectral densities (PSDs) measured by the EDP instrument in short bursts of 65536 samples/s when crossing the different regions of the reconnection layer that we identified above. Times of these waveforms are marked in Figure 2 by black arrows.

Figures 4a and 4b show 100 ms time intervals of the electric field E_y (in DE-spun spacecraft L vector coordinates) and their corresponding PSD measured around 14:46:58.7 UT, when MMS1 was in the separatrix region

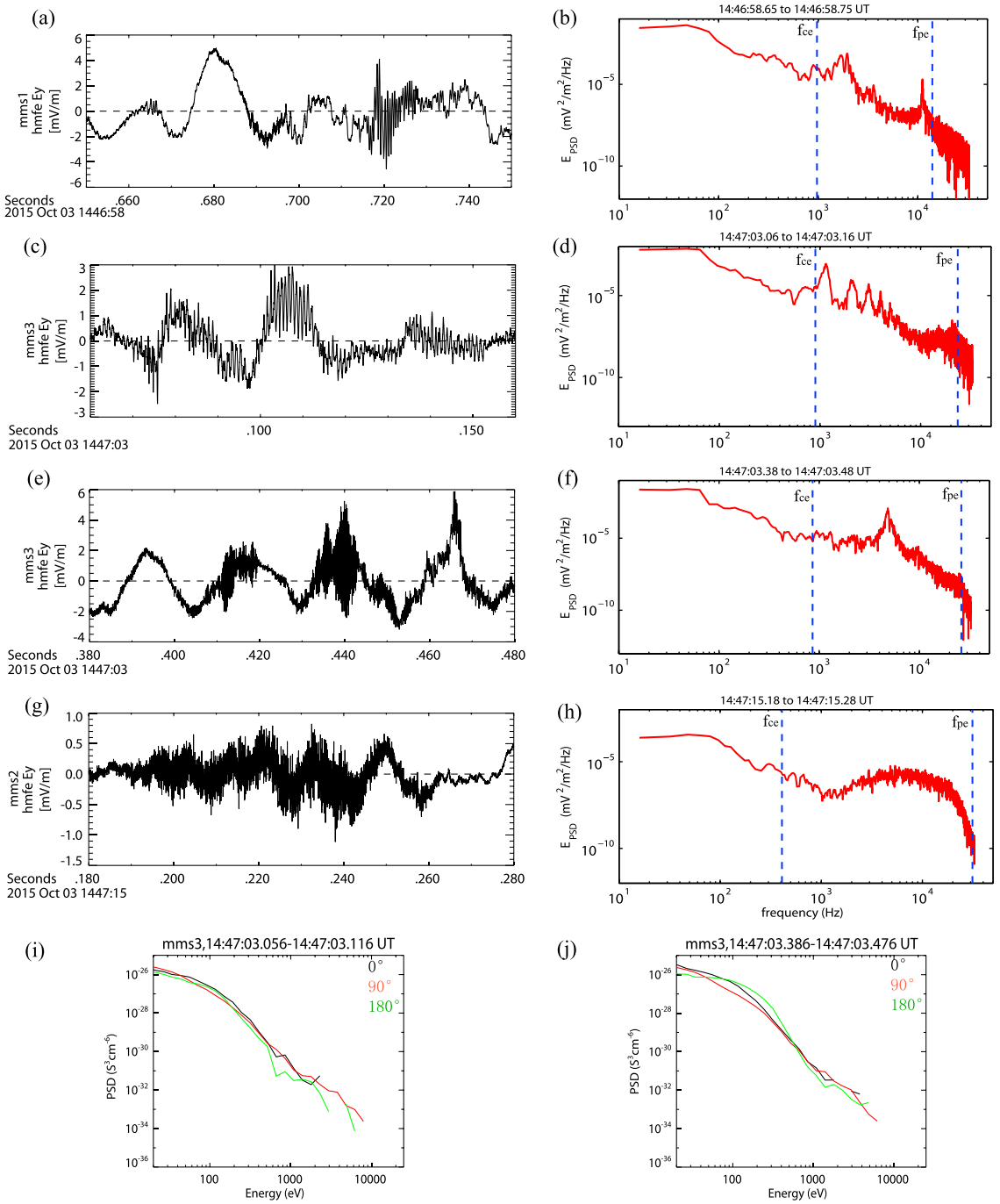

Figure 4. Observations of high-frequency waves and electron distributions around the ion diffusion regions. (a and b) *Y* component of electric field and the corresponding PSD at around 14:46:58.7 UT by MMS1, (c and d) 14:47:03.1 UT by MMS3, (e and f) 14:47:03.4 UT by MMS3, and (g and h) 14:47:15.2 UT by MMS2. PSDs were calculated by using fast Fourier transforms. Blue dashed lines in PSDs indicate f_{ce} and f_{pe}. (i and j) Electron pitch angle distributions corresponding to waves shown in Figures 4c and 4e. Black, red, and green traces represent the phase space densities of parallel (0°–30°), perpendicular (75°–105°), and antiparallel (150°–180°) electrons, respectively.

on the magnetosphere side. The maximum amplitudes of the waves were about 5 mV/m and did not show any associated magnetic field perturbations. Figure 4b shows two clear peaks in the PSD. One is located slightly above the electron gyrofrequency (f_{ce}) and the other is close to the electron plasma frequency (f_{pe}). Since the electric field perturbation of the electrostatic wave must be parallel to *k*, we analyzed their

Table 1. Energy Dissipation by the High-Frequency Waves in Different Regions of Reconnection Diffusion Region and Comparison to the Energy Dissipation by Lower-Frequency Process

	Time Interval (UT)	Dissipated Energy Density (10^{-9} J/m^3)
MP1 ($J \cdot E'$)	14:46:59–14:47:05	1.75
MP2 ($J \cdot E'$)	14:47:13–14:47:17	0.2
Waves on the magnetospheric separatrix ($J \cdot \delta E$)	14:46:57.9–14:46:59.8	−4.0e-5
Waves on the magnetosheath separatrix ($J \cdot \delta E$)	14:47:02.4–14:47:04.4	−3.6e-4
Waves in the MP current sheet ($J \cdot \delta E$)	14:47:13.9–14:47:15.7	1.2e-4

polarizations using the maximum variance analysis of the filtered electric field. The wave near f_{pe} is probably a Langmuir wave because the angle between the wave vector k and the ambient magnetic field B_0 $<k, B_0>$ was $5° \pm 2°$; i.e., it was field-aligned polarized. We found that wave at around 1.6 f_{ce} was also field-aligned polarized since $<k, B_0>$ was $12° \pm 2°$.

Figures 4c and 4d display the electric fields in a 100 ms time interval and the corresponding PSD near 14:47:03.1 UT, when MMS3 was in the separatrix region on the magnetosheath side. The PSD exhibits at least five clear peaks between f_{ce} and f_{pe}. These peaks are at frequencies of about 1150 Hz, 2100 Hz, 3050 Hz, 4000 Hz, and 5000 Hz. All these peaks are approximately the harmonics of 1150 Hz~1.27 f_{ce}. In addition, $<k, B_0>$ for these waves is $85° \pm 5°$. These indicate that they are electron cyclotron harmonic (ECH) waves. Figures 4e and 4f show the electric field and corresponding PSD at about 200 ms later than the waveform shown in Figure 4c. The PSD has a peak at around 4900 Hz, which is between f_{ce} and f_{pe}, while $<k, B_0>$ is $3° \pm 2°$. The ECH waves could have been generated by loss cone distribution or ring-like distribution [*Ashour-Abdalla and Kennel*, 1978; *Wong et al.*, 1991]. Figures 4i and 4j display two electron pitch angle distributions at the time of the waves shown in Figures 4c and 4e. Figure 4i shows a sudden decrease of antiparallel electron flux above 500 eV, which results in a loss cone distribution that probably excited the ECH waves. Such a loss cone distribution has been observed on the magnetospheric separatrix to explain the generation of whistler waves [*Graham et al.*, 2016] but has not been detected on the magnetosheath separatrix before. The waves shown in Figure 4e are consistent with a beam mode since Figure 4j displays a broad beam from ~30 eV extending to 500 eV. This beam is likely a combination of the accelerated magnetosheath electrons and the leakage of higher-energy magnetospheric electrons. In the presence of hot magnetospheric electrons and cold magnetosheath electrons, the free energy provided by beams could cause the electron acoustic mode to become unstable [*Ashour-Abdalla and Okuda*, 1986], which is plausibly the source of peaks in PSD as shown in Figures 4b and 4f. The changes of the wave mode and electron distributions in about 200 ms suggest that electron-scale physics is important in this region.

Figures 4g and 4h present the electric field and corresponding PSD at around 14:47:15.2 UT, when MMS2 was inside the current sheet. As in the previous case, the PSD exhibits a broad bump between f_{ce} and f_{pe}, and $<k, B_0>$ for this wave is $5° \pm 3°$, suggesting that it is either an electron beam mode or an electron acoustic wave.

6. Discussion and Summary

Contribution of these high-frequency waves to energy dissipation can be estimated by $J \cdot \delta E$ (here J is the DC current density computed from plasma moments while δE is the AC electric field that is high-pass filtered above the local f_{ce}). Using $J \cdot \delta E$ to estimate magnetic energy dissipation by plasma waves has been validated by *Wilson et al.* [2014]. Time series of $J \cdot \delta E$ contributed by the above analyzed high-frequency waves are shown in Figures 2f, 2g, and 2n. Although the amplitudes of $J \cdot \delta E$ are comparable to those of $J \cdot E'$, $J \cdot \delta E$ fluctuates frequently between negative and positive values. Table 1 lists the integrated energy density dissipated by these high-frequency waves and that through the lower-frequency electromagnetic fields $J \cdot E'$. The integrated energy dissipation per volume by high-frequency waves is at least 3 orders smaller than that by lower-frequency electromagnetic fields.

In summary, on 3 October 2015 MMS crossed the MP multiple times in the postnoon sector. Ion diffusion regions were identified during two ion-scale MP crossings by observations of Hall electromagnetic fields, slippage of ions with respect to the magnetic field, and magnetic energy dissipation. The dissipation regions were localized within the relatively thicker current sheet. High-frequency electrostatic waves between f_{ce} and f_{pe} were observed around the ion diffusion region. Field-aligned polarized waves were detected in the

separatrices on both sides of MP and within the MP current sheet, while electron cyclotron harmonic waves were observed in the magnetosheath separatrix. The field-aligned polarized waves are either electron beam modes or electron acoustic waves.

While previous studies have shown that the separatrices on the magnetosphere side are highly dynamic and structured regions with wave activity [*Retino et al.*, 2006], no significant waves had been observed in the magnetosheath separatrix region. For the first time we report the existence of ECH waves and electron beam modes in the magnetosheath separatrices. The high-resolution electromagnetic fields allow us to directly calculate the contribution to magnetic energy dissipation by these high-frequency waves. We find that these waves play negligible roles in converting energy from electromagnetic fields to plasma internal energy. Our results are an important contribution for understanding the role of high-frequency waves and electron dynamics during dayside magnetopause reconnection.

Acknowledgments
This research was supported by NASA Magnetospheric Multiscale Mission Interdisciplinary Scientist grant NNX08AO48G, NASA Heliospheric Grand Challenge grant NNX14AI16G, and NSF grant AGS-1450864. IRAP contribution to MMS was supported by CNES and CNRS. We thank the entire MMS team and instrument leads for data access and support. M.Z. appreciates D. Schriver and H.Y. Wei for their valuable discussions. The data presented in this paper are the L2 data of MMS and can be accessed from MMS Science Data Center (https://lasp.colorado.edu/mms/sdc/public/).

References

Ashour-Abdalla, M., and C. F. Kennel (1978), Nonconvective and convective electron cyclotron harmonic instabilities, *J. Geophys. Res.*, *83*(A4), 1531–1543, doi:10.1029/JA083iA04p01531.

Ashour-Abdalla, M., and H. Okuda (1986), Electron acoustic instabilities in the geomagnetic tail, *Geophys. Res. Lett.*, *13*, 366–369, doi:10.1029/GL013i004p00366.

Burch, J. L., T. E. Moore, R. B. Torbert, and B. L. Giles (2015), Magnetospheric Multiscale overview and science objectives, *Space Sci. Rev.*, doi:10.1007/s11214-015-0164-9.

Cassak, P. A., and M. A. Shay (2007), Scaling of asymmetric magnetic reconnection: General theory and collisional simulations, *Phys. Plasmas*, *14*, 102,114.

Dai, L. (2009), Collisionless magnetic reconnection via Alfvén eigenmodes, *Phys. Rev. Lett.*, *102*, 245003, doi:10.1103/PhysRevLett.102.245003.

Dai, L., C. Wang, V. Angelopoulos, and K.-H. Glassmeier (2015), In situ evidence of breaking the ion frozen-in condition via the non-gyrotropic pressure effect in magnetic reconnection, *Ann. Geophys.*, *33*, 1147–1153, doi:10.5194/angeo-33-1147-2015.

Deng, X. H., H. Matsumoto, H. Kojima, T. Mukai, R. R. Anderson, W. Baumjohann, and R. Nakamura (2004), Geotail encounter with reconnection diffusion region in the Earth's magnetotail: Evidence of multiple X lines collisionless reconnection?, *J. Geophys. Res.*, *109*, A05206, doi:10.1029/2003JA010031.

Dunlop, M. W., A. Balogh, K.-H. Glassmeier, and P. Robert (2002), Four-point Cluster application of magnetic field analysis tools: The curlometer, *J. Geophys. Res.*, *107*(A11), 1384, doi:10.1029/2001JA005088.

Ergun, R. E., et al. (2014), The axial double probe and fields signal processing for the MMS mission, *Space Sci. Rev.*, doi:10.1007/s11214-014-0115-x.

Goldman, M. V., D. L. Newman, and G. Lapenta (2015), What can we learn about magnetotail reconnection from 2D PIC Harris-sheet simulations?, *Space Sci. Rev.*, doi:10.1007/s11214-015-0154-y.

Graham, D. B., A. Vaivads, Y. V. Khotyaintsev, and M. Andre (2016), Whistler emission in the separatrix regions of asymmetric magnetic reconnection, *J. Geophys. Res. Space Physics*, *121*, 1934–1954, doi:10.1002/2015JA021239.

Lindqvist, P.-A., G. Olsson, R. B. Torbert, and B. King (2014), The spin-plane double probe electric field instrument for MMS, *Space Sci. Rev.*, doi:10.1007/s11214-014-0116-9.

Mozer, F. S., and F. L. Pritchett (2010), Electron physics of asymmetric magnetic field reconnection, *Space Sci. Rev.*, doi:10.1007/s11214-010-9681-8.

Pollock, C., et al. (2016), Fast plasma investigation for Magnetospheric Multiscale, *Space Sci. Rev.*, *199*, 331–406, doi:10.1007/s11214-016-0245-4.

Pritchett, P. L. (2008), Collisionless magnetic reconnection in an asymmetric current sheet, *J. Geophys. Res.*, *113*, A06210, doi:10.1029/2007JA012930.

Retinò, A., et al. (2006), Structure of the separatrix region close to a magnetic reconnection X-line: Cluster observations, *Geophys. Res. Lett.*, *33*, L06101, doi:10.1029/2005GL024650.

Russell, C. T., et al. (2014), The Magnetospheric Multiscale magnetometers, *Space Sci. Rev.*, doi:10.1007/s11214-014-0057-3.

Sonnerup, B. U. O., and M. Scheible (1998), Minimum and maximum variance analysis, in *Analysis Methods for Multi-Spacecraft Data*, edited by G. Paschmann and P. W. Daly, no. SR-001 in ISSI Scientific Reports, chap. 1, pp. 185–220, ESA Publ. Div., Noordwijk, Netherlands.

Sonnerup, B. U. O., S. E. Haaland, and G. Paschmann (2008), Discontinuity orientation, motion, and thickness, in *Multi-Spacecraft Analysis Methods Revisited*, edited by G. Paschmann and P. W. Daly, no. SR-008 in ISSI Scientific Reports, chap. 1, pp. 1-15, ESA Publ. Div., Noordwijk, Netherlands.

Tanaka, K. G., et al. (2008), Effects on magnetic reconnection of a density asymmetry across the current sheet, *Ann. Geophys.*, *26*, 2471.

Tang, X., C. Cattell, J. Dombeck, L. Dai, L. B. Wilson III, A. Breneman, and A. Hupach (2013), THEMIS observations of the magnetopause electron diffusion region: Large amplitude waves and heated electrons, *Geophys. Res. Lett.*, *40*, 2884–2890, doi:10.1002/grl.50565.

Torbert, R. B., et al. (2014), The FIELDS instrument suite on MMS: Scientific objectives, measurements, and data products, *Space Sci. Rev.*, doi:10.1007/s11214-014-0109-8.

Treumann, R. A. (2001), Origin of resistivity in reconnection, *Earth Planets Space*, *53*, 453–462.

Vaivads, A., Y. Khotyaintsev, M. Andre', A. Retino', S. C. Buchert, B. N. Rogers, P. De'cre'au, G. Paschmann, and T. D. Phan (2004), Structure of the magnetic reconnection diffusion region from four-spacecraft observations, *Phys. Rev. Lett.*, *93*(10), doi:10.1103/PhysRevLett.93.105001.

Viberg, H., Y. V. Khotyaintsev, A. Vaivads, M. André, and J. S. Pickett (2013), Mapping HF waves in the reconnection diffusion region, *Geophys. Res. Lett.*, *40*, 1032–1037, doi:10.1002/grl.50227.

Wilson, L. B., III, D. G. Sibeck, A. W. Breneman, O. Le Contel, C. Cully, D. L. Turner, V. Angelopoulos, and D. M. Malaspina (2014), Quantified energy dissipation rates in the terrestrial bow shock: 1. Analysis techniques and methodology, *J. Geophys. Res. Space Physics*, *119*, 6455–6474, doi:10.1002/2014JA019929.

Wong, H. K., M. L. Goldstein, and C. W. Smith (1991), Ion cyclotron harmonic resonances driven by ion ring-beam distributions, *J. Geophys. Res.*, *96*, 285–288, doi:10.1029/90JA02321.

Zhou, M., Y. Pang, X. H. Deng, Z. G. Yuan, and S. Y. Huang (2011), Density cavity in magnetic reconnection diffusion region in the presence of guide field, *J. Geophys. Res.*, *116*, A06222, doi:10.1029/2010JA016324.

Zhou, M., H. Li, X. Deng, S. Huang, Y. Pang, Z. Yuan, X. Xu, and R. Tang (2014), Characteristic distribution and possible roles of waves around the lower hybrid frequency in the magnetotail reconnection region, *J. Geophys. Res. Space Physics*, *119*, 8228–8242, doi:10.1002/2014JA019978.